Electric Power Systems Research 232 (2024) 110379

Contents lists available at ScienceDirect

Electric Power Systems Research

journal homepage: www.elsevier.com/locate/epsr

An integrated adequacy and stability assessment approach for microgrid reliability analysis under inverter-based resource contingency

Hadis Hosseinpour *, Mohammed Ben-Idris

Department of Electrical and Computer Engineering, Michigan State University, East Lansing, MI 48824, United States of America

ARTICLE INFO

Keywords:
Reliability assessment
Microgrid
Integrating adequacy and stability
Inverter-based resource (IBR)
Energy function

ABSTRACT

Power system reliability evaluation has been conducted based on steady-state analysis approaches such as optimal power flow calculations with minimum load curtailments. These approaches assume that a power system would return to a stable operating state after a contingency (faults, short circuits, etc.), i.e., power system dynamics are not considered. Although this assumption has been widely accepted for conventional power systems, microgrids are more vulnerable to large disturbances than conventional power systems are. In other words, the likelihood of an unstable transition from pre-event to post-event conditions is higher in the case of microgrids than in the case of conventional power grids. Therefore, it has become important to consider both generation adequacy and transient stability in microgrid reliability evaluation. This paper develops an integrated transient stability and reliability assessment approach for microgrids to capture both inadequacy and instability conditions. A Lyapunov function-based approach is developed to determine the stability region for each contingency in calculating the reliability indices. Also, a linearized AC optimal power flow model is developed for composite system reliability evaluation. This paper also provides a set of indices to quantify the impact of transient instability on the reliability of microgrids. The proposed approach is applied to the IEEE 33-bus system in the islanded mode using sedumi and YALMIP optimizers in MATLAB. The results show that 29.19% of the contingencies for which the microgrid is deemed reliable based on steady-state analyses causes unstable conditions, which justifies the need for integrating steady-state and transient conditions in microgrid reliability evaluation.

1. Introduction

Microgrids have been used in many applications including providing energy solutions to remote and isolated areas, operating electric ships, and enhancing the reliability of the power supply by the autonomous formation of localized microgrids. Assessing the reliability of microgrids is essential to quantify their value to these applications. Traditional reliability assessment methods for bulk power grids have been based on steady-state models with an underlying assumption that power grids can transit stably from one state to another (pre- and post-contingency conditions). However, this assumption ceases to be valid for the case of microgrids because microgrids are more vulnerable to small and large disturbances than large and interconnected power grids due to being small and isolated as well as having low inertia [1]. Therefore, it has become imperative to incorporate the dynamic responses of microgrids when evaluating their reliability. On the other hand, incorporating stability analysis in reliability studies is computationally involved due to the need to analyze a large set of contingencies for stability assessment. The development of direct methods for stability assessment has the potential to speed up the stability assessment.

The reliability of microgrids has been amply studied in the literature. Some reliability studies assume that microgrids and inverter-based distribution energy resources (DERs) can operate as small sources of active and reactive power or dispatchable units [2]. The complexity of microgrids and their potential lateral operating challenges have been modeled in the reliability assessment including customer impacts [3,4], different operation modes of microgrids [5,6], the challenges of PV reliability assessment [7], the uncertainty of renewable energy sources [8], and the effect of microgrid adoption on the reliability of distribution system and main utility [9,10]. The work in [3] has introduced the concept of the "virtual power plant" to model microgrids connected with intermittent sources in the reliability assessment. In [7], the uncertainty of renewable resources during the islanded operation mode has been modeled in the reliability assessment of microgrids. A three-level framework for assessing the reliability of distribution systems has

* Corresponding author.
E-mail addresses: hossei13@msu.edu (H. Hosseinpour), benidris@msu.edu (M. Ben-Idris).

https://doi.org/10.1016/j.epsr.2024.110379
Received 20 October 2023; Received in revised form 15 March 2024; Accepted 2 April 2024
Available online 11 April 2024

Nomenclature

$(.)_i$	The subscription for node i.
$P_i^{\text{Gen}}, Q_i^{\text{Gen}}$	Active & reactive power generation at node i.
$P_i^{\text{Gen,max (min)}}$	Maximum (minimum) active power generation at node i.
$Q_i^{\text{Gen,max (min)}}$	Maximum (minimum) reactive power generation at node i.
$P_i^{\text{load}}, Q_i^{\text{load}}$	Active & reactive power demand at node i.
$P_i^{\text{crtl}}, Q_i^{\text{crtl}}$	Active & reactive power curtailment at node i.
$P_{ij}^{\text{line}}, P_{ij}^{\text{line}}$	Active and reactive power flow through the line between nodes i and j.
$P_{ij}^{\text{loss}}, Q_{ij}^{\text{loss}}$	The active and reactive losses of the line between nodes i and j.
$\lvert V_i\rvert^{\text{max (min)}}$	Maximum (minimum) of voltage magnitudes at node i.
$\lvert Y_{ij}\rvert, \delta_{ij}$	Magnitude and angle of admittance matrix term in ith row to jth column.
G_{ij}, B_{ij}	Real and imaginary parts of admittance matrix term in ith row and jth column.
$\lvert V_i\rvert, \theta_i$	Magnitude and angle of voltage at node i.
$P_{e,i}^{\text{IBR}}, Q_{e,i}^{\text{IBR}}$	Active and reactive electric power injected into the network by IBR at node i
$P_{out,i}, Q_{out,i}$	The references of active and reactive power for IBR droop control at node i.
ω_i, ω_f	Angular velocity and low-pass filter frequency of IBR at node i.
$m_{p,i}, n_{q,i}$	P/f & Q/V droop control loop gains for IBR at node i.
v_{out}, ω_{out}	Output voltage and frequency of droop control.
$M_{P,i}, M_{Q,i}$	(Virtual) inertia constants of IBR at node i.
$M_{m,1}$, $D_{m,1}$	Inertia and damping constants of the synchronous generator at bus 1.
$D_{i,P}, D_{i,Q}$	(Virtual) damping constants of IBR at node i.
$\mathcal{V}_p, \mathcal{V}_k$	Potential and kinetic energy of system.

been proposed in [11], which accounts for the roles of both customers and distribution system operators.

Although several methods and techniques have been developed to improve the reliability evaluation of microgrids and inverters-based DERs, these methods evaluate the reliability of microgrids based on system adequacy without considering potential microgrid failures due to transient instabilities. System adequacy has been evaluated based on steady-state conditions, which assume the system is stable and voltage and frequency levels are within acceptable limits. In other words, existing methods do not consider potential system instability during the transition from pre-fault and post-fault conditions. However, transient stability assessment is essential to accurately evaluate system reliability by accounting for the potential instabilities during transient periods. By incorporating transient stability analysis into the system reliability evaluation process, a more reliable and robust assessment of the system's performance will be achieved.

A few studies [12–14], have integrated both the steady-state and transient conditions in the reliability assessment of power transmission systems where [14] is co-authored with Benidris. However, these approaches cannot be applied to microgrids due to the following factors: fast dynamic responses of microgrids introduced by inverter-based DERs, nonlinearity and complexity of dynamic models of power electronic devices utilized in inverter-based DERs, low inertia of microgrids, high R/X ratios of distribution lines, and unbalanced loads and power flows. As a result, traditional reliability assessment methods are no longer adequate, necessitating new approaches that take into account the unique characteristics of microgrids. It is necessary to analyze the system's transient response to changes and emerging scenarios, especially in the context of inverter-based DERs, owing to the rapid dynamics and intricate nature of their dynamic models. Incorporating the stability and reliability assessment for microgrids is, therefore, a research challenge that requires a comprehensive modeling of microgrid characteristics and the development of suitable analysis techniques.

This paper seamlessly integrates the assessment of reliability and the analysis of transient stability to comprehensively address the inadequacy and instability aspects of microgrids. The system's adequacy within each scenario is examined while scrutinizing the potential for a stable transition between any two scenarios. To facilitate accurate assessment, a linearized AC optimal power flow (AC-OPF) model has been devised and employed in conjunction with sequential Monte Carlo (SMC) simulation techniques to assess the adequacy of microgrids. In the realm of stability evaluation, a nonlinear transient energy function tailored for islanded microgrids has been developed, applying it to assess transient stability. The microgrid under investigation comprises five droop-controlled inverters and a synchronous generator. Within each scenario, the system's adequacy is explored through the application of a developed AC-OPF methodology in a linear programming problem. When the system adequately supplies its load demand, the reliability assessment proceeds to assess the feasibility of transitioning from the previous scenario to the subsequent one, employing the developed energy function for the stability evaluation.

The salient contributions of the study are outlined as follows:

- Developed an integrated framework for assessing the reliability of microgrids considering both inadequacy and transient instability aspects of microgrids.
- Developed a new transient energy function incorporating actual conditions in the distribution system. The energy function takes into account transfer conductance and the non-uniform virtual damping factor and inertia for grid-forming droop-controlled inverters, which is applicable for the transient stability assessment of large-scale microgrids and distribution systems.
- Introduced two system-wide stability–reliability indices and a unit-based reliability index to provide metrics that can assess the reliability and stability of microgrids. The utilization of unit-specific indices can help to discern the influence of each individual power system unit on the overall system's reliability. Moreover, stability–reliability indices provide valuable insights into the overall stability of the system and the degree of potential instability severity during unforeseen circumstances.

The rest of the paper is organized as follows. Section 2 presents reliability analysis and its constraint. Section 3 develops the energy function of the system and discusses the proposed stability constraint. In Section 4, the proposed approach is simulated, and the results are analyzed and discussed. Section 5 presents the conclusion.

2. Reliability analysis

DC optimal power flow models have been commonly used in power system reliability studies for determining minimum load curtailments due to contingencies. However, these models are inaccurate, especially for the distribution systems, due to the sensitivity of distribution systems to voltage variations and reactive power flows. For a more accurate reliability analysis for distribution systems and microgrids, voltage magnitudes and reactive power should be considered, which can be captured using AC-OPF models. However, AC-OPF models are computationally expensive, especially for studies that require repetitive

power flow solutions such as reliability studies. To address the problem of the poor accuracy of DC optimal power flow models and the computational burden of AC-OPF models, a linearized AC-OPF is applied to assess the system's inadequacy in this paper.

2.1. Linearized AC optimal power flow

In several studies [15,16], voltage angles have been ignored in linearized AC power flow models for distribution systems under the assumption that angle differences between adjacent nodes are small [17]. This assumption has been widely accepted for steady-state analyses of distribution systems.

However, deviations in voltage angles during contingencies impact energy and power flow in the system. Also, as detailed in Section 3.2.2, determining the steady-state operating point including voltage angles in each scenario is required for pre-event conditions in the transient stability assessment and characterizing the critical energy boundary. Consequently, preserving voltage angles in the linearized AC-OPF model is an indispensable part of the integrated reliability and stability assessment of microgrids. In this paper, a linearized AC power flow model for distribution systems that preserves voltage angles in addition to other variables is developed and applied for the integrated stability and reliability assessment. The development of the linearized optimal power flow model is explained as follows. The generally used active and reactive power balance equations at node i are as follows:

$$P_i^{\text{Gen}} + P_{e,i}^{\text{IBR}} = P_i^{\text{load}} + \sum_{j=1}^{b_i} P_{ij}^{\text{line}}\ , \quad Q_i^{\text{Gen}} + Q_{e,i}^{\text{IBR}} = Q_i^{\text{load}} + \sum_{j=1}^{b_i} Q_{ij}^{\text{line}}, \tag{1}$$

where b_i is the number of lines that leave node i. $\sum_{j=1}^{b_i} P_{ij}^{\text{line}}$ and $\sum_{j=1}^{b_i} Q_{ij}^{\text{line}}$ are denoted as P_i^{line} and Q_i^{line}. For the rest of the paper, $\theta_i - \theta_j$ is considered θ_{ij}. Assuming $Y_{ij} = G_{ij} + jB_{ij}$ (Y_{ij} is equal to $-y_{ij}$, which is the admittance of line between nodes i and j), P_i^{line} and Q_i^{line} can be expanded as follows,

$$P_i^{\text{line}} = G_{ii}|V_i|^2 + \sum_{j=1,j\neq i}^{b_i} |V_i|\,|V_j|\Big(G_{ij}\cos(\theta_{ij}) + B_{ij}\sin(\theta_{ij})\Big), \tag{2a}$$

$$Q_i^{\text{line}} = -B_{ii}|V_i|^2 + \sum_{j=1,j\neq i}^{b_i} |V_i|\,|V_j|\Big(G_{ij}\sin(\theta_{ij}) - B_{ij}\cos(\theta_{ij})\Big). \tag{2b}$$

Eqs. (2a) and (2b) are the general forms of active and reactive power flows, including the nonlinear terms. The nonlinearity of the power flow equations leads to increasing the computational time at each scenario in the adequacy assessment. Hence, by taking advantage of linearization techniques, a linearized AC power flow can be obtained.

In general, each of the active and reactive power flow equations has three nonlinear terms, including $|V_i|\,|V_j|\sin(\theta_{ij})$, $|V_i|\,|V_j|\cos(\theta_{ij})$, and $|V_i|^2$ as shown in (2). Since commonly assumed $\sin(\theta_i - \theta_j)$ or $\sin(\theta_{ij})$ is small, and the voltage is near 1.0 per unit, the first nonlinear term, $|V_i|\,|V_j|\sin(\theta_{ij})$, can be assumed to be equal to $|V_i||V_j|\sin(\theta_{ij}) = \theta_{ij} = \theta_i - \theta_j$. Substituting this assumption in (2a) and (2b), the $|V_i||V_j|\sin(\theta_{ij})$ term can be linearized.

At the next step, to linearize the $|V_i|\,|V_j|\cos(\theta_{ij})$ term in (2), the loss equations of line between nodes i and j are expanded and used [18]. By transposing loss equation terms on both equation sides and substituting the related terms, a linear expression for the $|V_i|\,|V_j|\cos(\theta_{ij})$ term can be obtained. The loss of the line between node i and node j is as follows:

$$P_{ij}^{\text{loss}} = \text{Re}\{(|V_i|\angle\theta_i - |V_j|\angle\theta_j)(|V_i|\angle\theta_i - |V_j|\angle\theta_j)^*(-Y_{ij}^*)\}, \tag{3a}$$

$$Q_{ij}^{\text{loss}} = \text{Im}\{(|V_i|\angle\theta_i - |V_j|\angle\theta_j)(|V_i|\angle\theta_i - |V_j|\angle\theta_j)^*(-Y_{ij}^*)\}. \tag{3b}$$

Substituting the complex expression of Y_{ij} in (3) and expanding them, P_{ij}^{loss} and Q_{ij}^{loss} can be expressed as follows:

$$P_{ij}^{\text{loss}} = -G_{ij}|V_i|^2 - G_{ij}|V_j|^2 + 2\,|V_i|\,|V_j|\,G_{ij}\ \cos(\theta_{ij}), \tag{4a}$$

$$Q_{ij}^{\text{loss}} = B_{ij}|V_i|^2 + B_{ij}|V_j|^2 - 2\,|V_i|\,|V_j|\,B_{ij}\ \cos(\theta_{ij}). \tag{4b}$$

Then, by transposing terms on both sides of (4a) and (4b), the equivalent to $|V_i|\,|V_j|\cos(\theta_{ij})$ term can be acquired for both active and reactive power flow as follows:

$$|V_i|\,|V_j|\ \cos(\theta_{ij}) = \frac{|V_i|^2 + |V_j|^2}{2} + \frac{P_{ij}^{\text{loss}}}{2G_{ij}}, \tag{5a}$$

$$|V_i|\,|V_j|\ \cos(\theta_{ij}) = \frac{|V_i|^2 + |V_j|^2}{2} - \frac{Q_{ij}^{\text{loss}}}{2B_{ij}}. \tag{5b}$$

Substituting (5) in (2), the power flow equation can be modified as follows:

$$P_i^{\text{line}} = G_{ii}|V_i|^2 + \sum_{j=1,j\neq i}^{b_i}\left(B_{ij}\ \theta_{ij} + G_{ij}\left[\frac{|V_i|^2 + |V_j|^2}{2} + \frac{P_{ij}^{\text{loss}}}{2G_{ij}}\right]\right), \tag{6a}$$

$$Q_i^{\text{line}} = -B_{ii}|V_i|^2 + \sum_{j=1,j\neq i}^{b_i}\left(G_{ij}\ \theta_{ij} - B_{ij}\left[\frac{|V_i|^2 + |V_j|^2}{2} - \frac{Q_{ij}^{\text{loss}}}{2B_{ij}}\right]\right). \tag{6b}$$

For more simplification in (6), the general definition of the main diameter of the admittance matrix needs to be substituted in the equations. So, according to the admittance matrix of the network, the real and imaginary parts in the main diameter of the admittance matrix are defined as follows,

$$G_{ii} = -\sum_{j=1,j\neq i}^{b_i} G_{ij}\ , \quad B_{ii} = -\sum_{j=1,j\neq i}^{b_i} B_{ij}. \tag{7}$$

Incorporating (7) in (6) and transposing terms in the equations, Eqs. (6a) and (6b) can be simplified as follows:

$$P_i^{\text{line}} = \frac{G_{ii}|V_i|^2}{2} + \sum_{j=1,j\neq i}^{b_i}\Big[B_{ij}\ \theta_{ij} + G_{ij}\Big(\frac{|V_j|^2}{2} + \frac{P_{ij}^{\text{loss}}}{2G_{ij}}\Big)\Big]. \tag{8a}$$

$$Q_i^{\text{line}} = -\frac{B_{ii}|V_i|^2}{2} + \sum_{j=1,j\neq i}^{b_i}\left(G_{ij}\ \theta_{ij} - B_{ij}\left[\frac{|V_j|^2}{2} - \frac{Q_{ij}^{\text{loss}}}{2B_{ij}}\right]\right). \tag{8b}$$

After linearizing the two terms of $|V_i|\,|V_j|\cos(\theta_{ij})$ and $|V_i|\,|V_j|\sin(\theta_{ij})$, the $|V_i|^2$ term needs to be linearized. If $f(|V_i|)$ is defined as (9), according to the Taylor series, $|V_i^2|$ can be approximated as follows [18]:

$$\begin{aligned} f(|V_i|) = |V_i|^2 \to f(|V_i|) \cong f(1) + \left.\frac{\mathrm{d}f}{\mathrm{d}|V_i|}\right|_{|V_i|=1}.(|V_i| - 1) \to |V_i|^2 \cong 1 \\ + 2(|V_i| - 1) = 2|V_i| - 1. \end{aligned} \tag{9}$$

Applying the Taylor approximation, expanding θ_{ij} to $\theta_i - \theta_j$, and substituting (7) in (8a) and (8b), the active and reactive power flow equations can be modified as follows:

$$\begin{aligned} P_i^{\text{line}} &= \frac{G_{ii}(2|V_i| \not{-1})}{2} + \sum_{j=1,j\neq i}^{b_i}\left(B_{ij}\theta_{ij} + G_{ij}\left[\frac{(2|V_j| \not{-1})}{2} + \frac{P_{ij}^{\text{loss}}}{2G_{ij}}\right]\right) \\ &= G_{ii}|V_i| + \sum_{j=1,j\neq i}^{b_i}\left(B_{ij}\overset{(\theta_i - \theta_j)}{\not{\theta}_{ij}} + G_{ij}|V_j| + \frac{P_{ij}^{\text{loss}}}{2}\right), \end{aligned} \tag{10}$$

where the constant (-1)s in each equation are canceled based on (7). By expanding $\sum_{j=1,j\neq i}^{b_i} B_{ij}(\theta_i - \theta_j)$ into $(\theta_i \sum_{j=1,j\neq i}^{b_i} B_{ij})$ and $(-\sum_{j=1,j\neq i}^{b_i} B_{ij}\theta_j)$ as well as substituting (7) in $(\theta_i \sum_{j=1,j\neq i}^{b_i} B_{ij})$, Eq. (10) can be simplified as follows:

$$P_i^{\text{line}} = G_{ii}|V_i| - B_{ii}\theta_i + \sum_{j=1,j\neq i}^{b_i}\left(-B_{ij}\theta_j + G_{ij}|V_j| + \frac{P_{ij}^{\text{loss}}}{2}\right). \tag{11}$$

The same assumptions exerted in (10) and (11) can be applied to simplify the reactive power flow equation as follows:

$$Q_i^{\text{line}} = -B_{ii}|V_i| - G_{ii}\theta_i + \sum_{j=1,j\neq i}^{b_i}\left(-G_{ij}\theta_j - B_{ij}|V_j| + \frac{Q_{ij}^{\text{loss}}}{2}\right). \tag{12}$$

Although P_{ij}^{loss} and Q_{ij}^{loss} are the nonlinear terms in AC power flow, the line losses are very small compared to other terms, and in reliability and stability analysis, the P_{ij}^{loss} and Q_{ij}^{loss} can be neglected [19]. The Eqs. (11) and (12) can be modified as follows:

$$\mathbf{P}^{\text{line}} = \mathbf{G}\mathbf{V} - \mathbf{B}\Theta, \quad \mathbf{Q}^{\text{line}} = -\mathbf{B}\mathbf{V} - \mathbf{G}\Theta, \tag{13}$$

where $\mathbf{G}$ and $\mathbf{B}$ are real and imaginary terms of the grid admittance matrix such that $\mathbf{Y} = \mathbf{G} + j\mathbf{B}$. The other parameters in (13) are listed as follows:

$$\mathbf{P}^{\text{line}} = \begin{bmatrix} P_1^{\text{line}} \\ \dots \\ P_n^{\text{line}} \end{bmatrix}, \mathbf{Q}^{\text{line}} = \begin{bmatrix} Q_1^{\text{line}} \\ \dots \\ Q_n^{\text{line}} \end{bmatrix}, \mathbf{V} = \begin{bmatrix} |V_1| \\ \dots \\ |V_n| \end{bmatrix}, \Theta = \begin{bmatrix} \theta_1 \\ \dots \\ \theta_n \end{bmatrix}. \tag{14}$$

2.2. Optimization problem

To optimize the power flow problem, minimizing the sum of load curtailments of the grid is defined as the objective function of the linear programming problem as follows:

$$\text{Objective function: } P_{grid}^{\text{crtl}} = \min \sum_{i=1}^{n} P_i^{\text{crtl}}, \tag{15}$$

where n is the number of nodes; and P_{grid}^{crtl} present the total load curtailment in each scenario. The linear AC-OPF problem is subjected to the following constraints:

$$P_i^{\text{Gen}} + P_{e,i}^{\text{IBR}} + P_i^{\text{crtl}} - P_i^{\text{load}} - P_i^{\text{line}} = 0, \tag{16a}$$

$$Q_i^{\text{Gen}} + Q_{e,i}^{\text{IBR}} + Q_i^{\text{crtl}} - Q_i^{\text{load}} - Q_i^{\text{line}} = 0, \tag{16b}$$

where P_i^{Gen}, Q_i^{Gen}, $P_{e,i}^{\text{IBR}}$, $Q_{e,i}^{\text{IBR}}$, P_i^{crtl}, and Q_i^{crtl} are the decision variables for addressing the linear programming problem. Moreover, according to definition of P_i^{line} and Q_i^{line} in (13), the magnitude and angle of voltages are also the decision variables for minimizing load curtailments. P_1^{Gen} and Q_1^{Gen} contain the real and reactive power supplied by the synchronous generator at node 1, respectively. The other constraints of decision variables required to address the linear programming problem are enumerated and elaborated upon as follows:

$$P_i^{\text{Gen,min}} \le P_i^{\text{Gen}} \le P_i^{\text{Gen,max}}, \tag{17a}$$

$$Q_i^{\text{Gen,min}} \le Q_i^{\text{Gen}} \le Q_i^{\text{Gen,max}}, \tag{17b}$$

$$P_{e,i}^{\text{IBR,min}} \le P_{e,i}^{\text{IBR}} \le P_{e,i}^{\text{IBR,max}}, \tag{17c}$$

$$Q_{e,i}^{\text{IBR,min}} \le Q_{e,i}^{\text{IBR}} \le Q_{e,i}^{\text{IBR,max}}, \tag{17d}$$

$$|V_i|^{\text{min}} \le |V_i| \le |V_i|^{\text{max}}, \tag{17e}$$

$$\theta_i \quad \text{unrestricted}, \tag{17f}$$

$$0 \le P_i^{\text{crtl}} \le P_i^{\text{load}}, \tag{17g}$$

$$0 \le Q_i^{\text{crtl}} \le Q_i^{\text{load}}, \text{ such that } Q_i^{\text{crtl}} = P_i^{\text{crtl}} \left(\frac{Q_i^{\text{load}}}{P_i^{\text{load}}} \right). \tag{17h}$$

The active and reactive powers of a distributed generator are limited by (17g) and (17d), respectively. The voltage magnitude and angle are confined by (17e). The allowable load curtailment is defined by (17h).

2.3. Reliability indices

In the proposed method, the system instability and inadequacy in each scenario are investigated and illustrated through the reliability indices. The System Average Interruption Duration Index (SAIDI) and System Average Interruption Frequency Index (SAIFI) capture system inadequacy to meet load demand. In the instability evaluation, the possibility of transition from the previous steady-state operating point to another point is determined based on the energy function of the whole system, such that if the system is stable, the scenario is defined as a *"successful"* scenario; otherwise, it is defined as a *"failure"* scenario. In case of instability, the entire load is lost. Therefore, in an unstable transition, the amount of load curtailment is the hourly load peak based on the load profile. Hence, based on the stability framework, Loss of Load Probability (LOLP), Loss of Load Expectation (LOLE), Loss of Load Frequency (LOLF), Expected Demand Not Served (EDNS), and Expected Energy Not Served (EENS) are also considered here to evaluate and compare the probability, frequency, and intensity of unstable and inadequate scenarios. Although the LOLP, LOLE, LOLF, EDNS, and EENS indices have been traditionally used for transmission systems, we use them for microgrids to emphasize system failures as opposed to customer-oriented indices such as SAIDI and SAIFI.

2.3.1. System Average Interruption Duration Index (SAIDI)

The SAIDI measures the annual average time of power supply interruptions per customer.

$$\text{SAIDI} = \sum_{j=1}^{N} \frac{\Psi_j^{hr.int}}{\Psi_j} \times 8760 \quad \text{(h/cus.yr)}, \tag{18}$$

where N is the number of scenarios; $\Psi_j^{hr.int}$ is the duration of sustained customer interruptions in Scenario j in hours; and Ψ_j is the total number of customers in Scenario j.

2.3.2. System Average Interruption Frequency Index (SAIFI)

The SAIFI provides a measure for the annual average number of outages per customer.

$$\text{SAIFI} = \sum_{j=1}^{N} \frac{\Psi_j^{occ.int}}{\Psi_j} \times 8760 \quad \text{(occ/cus.yr)}, \tag{19}$$

where $\Psi_j^{occ.int}$ is the number of sustained customer interruptions in Scenario j.

2.3.3. Loss of Load Probability (LOLP)

The LOLP is the probability of encountering one or more loss of load events during a given period of time. Using the sequential Monte Carlo simulation, the LOLP can be calculated as follows,

$$\text{LOLP} = \sum_{j=1}^{N} \frac{F_j}{N} \quad \text{such that} \quad \begin{cases} \text{In failure scenario: } F_j = 1 \\ \text{In success scenario: } F_j = 0 \end{cases}. \tag{20}$$

2.3.4. Loss of Load Expectation (LOLE)

LOLE represents the expected (average) number of hours in which the load exceeds the available generation capacity during a specified period. It is calculated by multiplying the LOLP by the total number of hours in the assessment period such that LOLE = LOLP × 8760 (h/yr).

2.3.5. Loss of Load Frequency (LOLF)

The LOLF is the average number of transitions from success to failure states or vice versa. The LOLF can be calculated using sequential Monte Carlo simulation as follows,

$$\text{LOLF} = \sum_{j=1}^{N} \frac{T_j^{SF}}{N} \times 8760 \quad \text{(occ/yr)}, \tag{21}$$

where T_j^{SF} equals 1 if the system state changes from a success state to a failure state; otherwise, T_j^{SF} equals 0.

2.3.6. Expected Demand Not Served (EDNS)

The EDNS index is the anticipated (average) demand that the system is unable to meet during a specific time frame due to loss of load occurrences, which is calculated as follows:

$$\text{EDNS} = \sum_{j=1}^{N} \frac{P_{grid,j}^{\text{crtl}}}{N} \quad \text{(MW)}, \tag{22}$$

where $P_{grid,j}^{\text{crtl}}$ represents the curtailment in Scenario j in MW.

2.3.7. Expected Energy Not Served (EENS)

Focuses on the expected (average) amount of energy that is not supplied during power interruptions. It is calculated by multiplying the EDNS by the total number of hours in the assessment period, such that EENS = EDNS × 8760 (MWh).

2.3.8. Unit Impact on System Unreliability (UISUR)

A new proposed index in this study is the unit impact on system unreliability (UISUR). The UISUR index presents the effect of each unit on network reliability. The UISUR of unit z is defined as follows:

$$\text{UISUR}_z = \sum_{f=1}^{M} \frac{\xi_{f,z}^{\text{fail}}}{M}, \tag{23}$$

where M is the number of failure scenarios, and $\xi_{f,z}^{\text{fail}}$ is the state of unit z at fth failure scenario such that if the unit z is failed, $\xi_{f,z}^{\text{fail}}$ is equal to 1; otherwise, it is equal to 0. The UISUR index can help to identify the more operationally effective units (or devices) in the unreliability of the network and determine the weak points in the network. The UISUR can be generally defined for all devices and equipment in the grid that are susceptible to failure or outage, such as generators, lines, inverter-based resources (IBRs), DERs, and switches. The UISUR index is a helpful criterion for any purpose of future planning.

3. Transient stability analysis

For stability analysis, it is essential to find a well-developed dynamic model of the grid with well-reasoned simplifications as well as a systematic and time-efficient stability analysis method. In this study, a second-order model is used to model the dynamics of IBRs (discussed in Section 3.1). To address the transient stability assessment, the energy function is developed based on the nonlinear dynamic model (discussed in Section 3.2), and the potential energy boundary surface method is applied as the stability analysis method.

3.1. Background on microgrid dynamic models

Microgrids and IBRs include a variety of control systems and power electronic devices that must be considered in the microgrid dynamic model to have a sufficiently realistic and accurate assessment in both reliability and stability evaluations. A detailed model suffers from the problems of the time-consuming computational process [20]. Moreover, applying a meticulous dynamic model in reliability evaluation adds another level of complexity and intensifies the problem of the computational burden. On the contrary, applying extreme simplifications of the dynamic model with excessive approximations cannot result in a trustworthy and authentic stability and reliability assessment.

In the existing approaches for transient stability assessment and power system dynamics appraisal, two dynamic models of IBRs are widely applied for large-signal analysis including the full-order (or reduced-order) time-domain dynamics and the second-order (or virtual synchronous generator (VSG)) [20,21] models. Although the high-order time-domain dynamic models of IBRs provide precise dynamics of the network, the stability and reliability analyses based on this model are computationally cumbersome. On the other hand, the second-order model presents an IBR as a synchronous generator. The simplicity and ease with which the second-order model or VSG model of IBRs can be employed in assessing stability and reliability are matched by its acceptable level of accuracy. The analyses provided in [22,23] reveal the reliability of the VSG model. These findings underscore the VSG model's effectiveness in enabling a comprehensive and robust adequacy and stability evaluation of IBRs and microgrids.

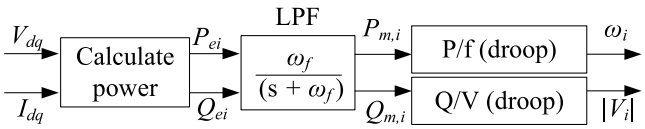

Fig. 1. The droop control of a grid-forming inverter-based resource.

3.1.1. Dynamic model of inverter-based resources

The dynamic model of a system must represent the system's behavior with an acceptable level of accuracy. In this study, the virtual synchronous generator model is applied as the dynamic model of IBRs. In this model, the dynamic behavior of IBRs is treated like a synchronous machine, defining a new equivalent damping factor and a new equivalent inertia for each IBR. Based on the droop regulators of a grid-forming droop-controlled inverter shown in Fig. 1, low-pass filters and droop control model are as follows:

$$\omega_i = \omega_{out} - m_{p,i}\,(P_{m,i} - P_{out,i})\,,\quad P_{m,i} = (\omega_f P_{e,i}^{\text{IBR}})/(s+\omega_f)\,,\quad \forall\ P_{e,i}^{\text{IBR}} = V_q I_{oq} + V_d I_d, \tag{24a}$$

$$|V_i| = v_{out} - n_{q,i}\,(Q_{m,i} - Q_{out,i})\,,\quad Q_{m,i} = (\omega_f Q_{e,i}^{\text{IBR}})/(s+\omega_f)\,,\quad \forall\ Q_{e,i}^{\text{IBR}} = V_d I_q - V_q I_d. \tag{24b}$$

The microgrid droop control system, as described in [21,24], mimics the inertia and damping features of synchronous machines. This is achieved by formulating their resemblance through the following equation [24]:

$$\omega_i = \omega_{out} - m_{p,i}\left(\frac{\omega_f}{s+\omega_f} P_{e,i}^{\text{IBR}} - P_{out,i}\right) \rightarrow P_{e,i}^{\text{IBR}} = \left(\frac{s}{\omega_f} + 1\right) \times \left(\frac{1}{m_{p,i}}(\omega_{out} - \omega_i) + P_{out,i}\right). \tag{25}$$

Utilizing (24a), the aforementioned P/f control loop can be written as follows:

$$\frac{1}{\omega_f m_{p,i}} s\,\omega_i = P_{out,i} - P_{e,i}^{\text{IBR}} - \frac{1}{m_{p,i}}(\omega_i - \omega_{out}) \rightarrow \frac{1}{\omega_f m_{p,i}}\dot{\omega}_i = P_{out,i} - P_{e,i}^{\text{IBR}} - \frac{1}{m_{p,i}}(\omega_i - \omega_{out}). \tag{26}$$

By comparing the derived expression is (26) with the typical definition of the swing equation used for synchronous generators, the damping rate and virtual inertia values of IBRs can be established. Specifically, they can be defined as follows:

$$D_{i,P} = (m_{p,i})^{-1}\,,\quad M_{P,i} = (\omega_f\, m_{p,i})^{-1}. \tag{27}$$

For the reactive power and voltage (Q/V) control loop equation, by applying the same process, the dynamic model can be represented as follows:

$$\frac{1}{\omega_f n_{q,i}}|\dot{V}_i| = Q_{out,i} - Q_{e,i}^{\text{IBR}} - \frac{1}{n_{q,i}}(|V_i| - v_{out}) \Rightarrow\ D_{i,Q} = (n_{q,i})^{-1}\,,\quad M_{Q,i} = (\omega_f\, n_{q,i})^{-1}. \tag{28}$$

As the dynamic response of the controlling system and power electronics devices is fast, the v_{out} and ω_{out} can be considered equal to $|V_i|$ and ω_i, respectively. Consequently, an IBR can be modeled using (29).

$$M_{P,i}\,\dot{\omega}_i + D_{i,P}\,\Delta\omega_i = P_{out,i} - P_{e,i}^{\text{IBR}}\,,\quad \frac{\partial\theta_i}{\partial t} = \omega_i, \tag{29a}$$

$$M_{Q,i}\,|\dot{V}_i| + D_{i,Q}\,\Delta|V_i| = Q_{out,i} - Q_{e,i}^{\mathrm{IBR}},\ i = 1, 2, \ldots, n. \tag{29b}$$

In addition to a suitably simplified dynamic model of the network, an uncomplicated and efficient approach to assessing the transient stability and dynamics of microgrids is indispensable. In the following section, an energy function, including the presented dynamic model of IBRs, is developed for the transient stability studies.

3.2. Stability assessment and energy function

Generally, two main system stability assessment methods exist, which are time-domain simulation and direct methods. Although the time-domain simulation method offers a meticulous evaluation of the system's dynamic response, it is a laborious and convoluted task that consumes significant amounts of time and effort due to simulating each scenario as a new case study because, for each new scenario, the system needs to be simulated meticulously in software to analyze the scenario dynamic. In contrast, direct methods provide a general mathematical model of the system, representing the system dynamic in each scenario, and the stability of the system can be analyzed. So, direct methods are time-efficient methods and provide stability indices, e.g., energy margin. Not only does the energy margin provide an index for system stability, but it also provides a measure for system level of stability, i.e., a large positive value means the system is highly stable and vice versa.

There have been a great number of stability perusals on the direct methods including the transient energy (TE) Method [25], the Kyoto method [26], and the acceleration approach [27] improved the accuracy of stability analysis. The hyperplane method [28] considers more accurate electrical machine models and transfer conductances. The work in [29] has provided a general and precise energy function for a multi-machine system for transient stability assessment. All aforementioned methods are classified as scalar Lyapunov functions and present a system-based stability assessment for a transmission-level power system.

3.2.1. Transient energy function

For the stability assessment of the simulated scenarios, the transient stability assessment in each scenario is analyzed using an energy function method and the maximum potential energy boundary. Generally, each system has an energy function, including potential and kinetic energies. The critical and clearing energies must be calculated and analyzed for transient stability assessment. Specifically, the critical energy boundary sets the upper limit on the energy level that the system can withstand during a disturbance trajectory to ensure a stable transition to the original steady-state operation or equilibrium point. The clearing energy represents the energy level of the system when the fault or contingency is cleared. By employing this energy-based approach, a comprehensive analysis of the system's stability can be performed, enabling the identification of potential instability scenarios and the development of appropriate mitigation strategies.

In this study, the critical energy boundary is equal to the maximum potential energy that the system can have. The clearing energy is defined as the system energy level when the disturbance is cleared. To have a stable transition to the steady-state operating point, the clearing energy must be less than the critical energy. For investigation on the feasibility of a stable transition, a precise energy function of the system must be developed that can present the dynamic behavior of the system in each situation, including pre-, during, and post-fault conditions.

3.2.2. Formulating an energy function

To find the energy function of the system, it is necessary to obtain the active and reactive power equations of the system during the disturbance and integrate them over the disturbance time interval including from the time operation leaves the steady-state operating point to the disturbance-clearing time or integral over the variable change during the disturbance time (the variable that depends on the time). According to [29], the active and reactive power equations can be defined as follows:

$$P_i := -P_i^{\mathrm{Gen}} - P_{e,i}^{\mathrm{IBR}} + P_i^{\mathrm{load}} + \sum_{j=1}^{b_i} P_{ij}^{\mathrm{line}} := \frac{d\,\mathcal{U}(|V|,\theta)}{d\theta_i} \tag{30a}$$

$$Q_i := \left[-Q_i^{\mathrm{Gen}} - Q_{e,i}^{\mathrm{IBR}} + Q_i^{\mathrm{load}} + \sum_{j=1}^{b_i} Q_{ij}^{\mathrm{line}}\right]/|V_i| := \frac{d\,\mathcal{U}(|V|,\theta)}{d|V_i|}, \tag{30b}$$

where $\mathcal{U}(|V|,\theta)$ indicates the energy function. Considering the swing equation for the synchronous generator at node 1 (i.e. $M_{m,1}\ \dot{\omega}_m + D_{m,1}\ \Delta\omega_m = P_{m,1}^{\mathrm{Gen}} - P_1^{\mathrm{Gen}}$), (2a), (2b), and (29), integrating (30a) and (30b) over the time, and collecting all energy terms, the transient energy function is defined based on the nonlinear AC power flow as follows:

$$\mathcal{U}_1 = -P_{m,1}^{\mathrm{Gen}}\,(\theta_1 - \theta_{01}^s) - \sum_{i=1}^{n} P_{out,i}\,(\theta_i - \theta_{0i}^s), \tag{31a}$$

$$\mathcal{K}_1 = \frac{1}{2} M_{m,1}\,\omega_m^2 + \frac{1}{2}\sum_{i=1}^{n} M_{P,i}\,\omega_i^2, \tag{31b}$$

$$\mathcal{U}_2 = \sum_{i=1}^{n}\int_{\theta_{0i}^s}^{\theta_i} P_i^{\mathrm{load}}\,d\theta_i = \sum_{i=1}^{n} P_i^{\mathrm{load}}\,(\theta_i - \theta_{0i}^s), \tag{31c}$$

$$\begin{aligned}\mathcal{U}_3 &= \sum_{i=1}^{n}\int_{\theta_{0i}^s}^{\theta_i}\sum_{j=1}^{n}|V_i|\,|V_j|\Big(B_{ij}\sin(\theta_{ij}) + G_{ij}\cos(\theta_{ij})\Big)d\theta_i \\ &= \sum_{i=1}^{n}|V_i|^2\,G_{ii}(\theta_i - \theta_{0i}^s) \\ &+ \sum_{i=1}^{n}\sum_{j\neq i}^{n}|V_i|\,|V_j|\Big((-B_{ij}\cos(\theta_{ij}) + G_{ij}\sin(\theta_{ij})) - (-B_{ij}\cos(\theta_{0i}^s - \theta_j) \\ &+ G_{ij}\sin(\theta_{0i}^s - \theta_j))\Big),\end{aligned} \tag{31d}$$

$$\begin{aligned}\mathcal{U}_4 &= -\int_{|V_{01}^s|}^{|V_1|}\frac{Q_1^{\mathrm{Gen}}}{|V_1|}\,d|V_1| - \sum_{i=1}^{n}\int_{|V_{0i}^s|}^{|V_i|}\frac{Q_{out,i}}{|V_i|}\,d|V_i| \\ &= -Q_1^{\mathrm{Gen}}\left(\ln(|V_i|) - \ln(|V_{0i}^s|)\right) - \sum_{i=1}^{n} Q_{out,i}\left(\ln(|V_i|) - \ln(|V_{0i}^s|)\right),\end{aligned} \tag{31e}$$

$$\mathcal{K}_2 = \sum_{i=1}^{n} M_{Q,i}\left(\ln(|V_i|) - \ln(|V_{0i}^s|)\right), \tag{31f}$$

$$\mathcal{U}_5 = \sum_{i=1}^{n}\int_{|V_{0i}^s|}^{|V_i|}\frac{Q_i^{\mathrm{load}}}{|V_i|}\,d|V_i| = \sum_{i=1}^{n} Q_i^{\mathrm{load}}\left(\ln(|V_i|) - \ln(|V_{0i}^s|)\right), \tag{31g}$$

$$\begin{aligned}\mathcal{U}_6 &= \sum_{i=1}^{n}\int_{|V_{0i}^s|}^{|V_i|}\sum_{j=1}^{n}|V_j|(G_{ij}\sin(\theta_{ij}) - B_{ij}\cos(\theta_{ij}))\,d|V_i| \\ &= -\sum_{i=1}^{n}(|V_i|^2 - |V_{0i}^s|^2)B_{ii} + \sum_{i=1}^{n}\sum_{j\neq i}^{n}|V_j|\Big(|V_i| - V_{0i}^s|\Big) \\ &\times \Big(G_{ij}\sin(\theta_{ij}) - B_{ij}\cos(\theta_{ij})\Big).\end{aligned} \tag{31h}$$

As mentioned before, the energy function is constructed by two terms, which are kinetic energy, $\mathcal{V}_k(|V|,\theta)$, and potential energy, $\mathcal{V}_p(|V|,\theta)$, which are expressed as follows:

$$\begin{aligned}\mathcal{V}_k(|V|,\theta) = \mathcal{K}_1 + \mathcal{K}_2 &= \frac{1}{2}M_{m,1}\,\omega_m^2 + \frac{1}{2}\sum_{i=1}^{n} M_{P,i}\,\omega_i^2 \\ &+ \sum_{i=1}^{n} M_{Q,i}\Big(\ln(|V_i|) - \ln(|V_{0i}^s|)\Big),\end{aligned} \tag{32a}$$

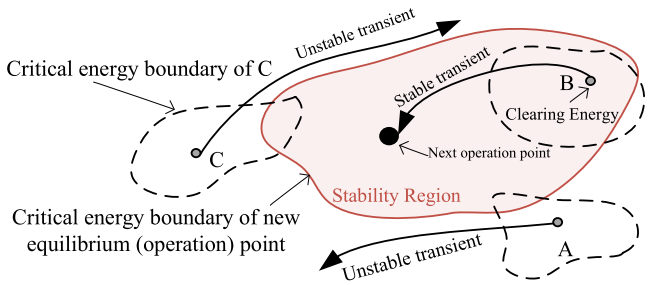

Fig. 2. Critical energy boundary and transient stability.

$$\mathcal{V}_p(|V|,\theta) = \sum_{j=1}^{6} \mathcal{U}_j, \tag{32b}$$

where $(.)^s_{0i}$ indicates the parameter stable equilibrium point. $M_{P,i}$ and $M_{Q,i}$ are determined for IBR at node i based on (27) and (28). The derivative of the energy function is as follows:

$$\dot{\mathcal{V}}(|V|,\theta) = \dot{\mathcal{U}}(|V|,\theta) = \dot{\mathcal{V}}_p(|V|,\theta) + \dot{\mathcal{V}}_k(|V|,\theta), \tag{33a}$$

$$\dot{\mathcal{V}} = -D_{m,1}\,\Delta\omega_m - \sum_{i=1}^{n} D_{i,P}\,\Delta\omega_i - \sum_{i=1}^{n} D_{i,Q}\,\Delta|V_i|. \tag{33b}$$

The proposed energy function in Section 3.2.2 is suitable for use in assessing DERs, grid-forming IBRs, generators in transmission and distribution systems, and any network following the swing equations as their dynamic model.

3.2.3. Critical energy boundary

To guarantee a stable transition in each scenario, the clearing energy must be less than the critical energy, as follows:

$$\Delta\mathcal{V}\,(|V^s_{0i}|,\theta^s_{0i}) = \mathcal{V}^{\text{critical}} - \mathcal{V}^{\text{clearing}} > 0\,, \tag{34}$$

where $\mathcal{V}^{\text{critical}}$ and $\mathcal{V}^{\text{clearing}}$ are the critical and clearing energy boundaries, respectively. During the sequential Monte Carlo process, each scenario is considered a new disturbance, and the system should move to a new steady-state operating point calculated by linear AC-OPF in the adequacy assessment section. Table 6 (in the Appendix) presents the effect of using the equilibrium point constructed using the linear AC-OPF compared with the nonlinear AC-OPF on the accuracy of the calculated energy boundaries. Using the transient energy function, Eq. (34) evaluates whether this transition from the previous equilibrium point to the new operating point as the new equilibrium point is possible. This study obtains the critical energy boundary by maximizing the potential energy [30]. The critical energy boundary is the local maximum around the equilibrium point.

Eq. (34) guarantees a stable transition to the new equilibrium point in each scenario; otherwise, the transition is considered unsuccessful. For the stability assessment of each sampled system transition, the current operating point is considered as the system state at clearing time, and the grid dynamics need to return to its equilibrium point, i.e., the new next steady-state operating point obtained by the optimal power flow. The clearing energy and critical energy boundary are computed based on the states and the grid conditions at the current operating point and next operating point, respectively. The term *"grid status"* refers to the voltage magnitudes and angles of the system $(|V_{i-1}|,\theta_{i-1})$, and the term *"grid conditions"* refers to the hourly loads and the operating states of IBRs, which determine which ones are functioning properly and which ones have failed.

If the clearing energy level is less than the critical energy boundary, the grid experiences a successful transition to the next steady-state operating point and vice versa. In Fig. 2, the current steady-state operating points A and C suffer from transient instability due to the larger energy level compared to the critical energy boundary of the next steady-state operating point. However, the transition from the current steady-state operating point B to the next operating point is stable, guaranteeing a *"successful"* scenario.

Table 1
The reliability information of IBRs.

Node	Active power (MW)	Reactive power (MVAR)	MTTF (h/yr)	MTTR (h/yr)
11	0.3	0.25	7410	1350
18	0.25	0.25	7234	1526
22	0.2	0.2	7538	1222
25	0.25	0.25	6612	2148
33	0.2	0.2	8085	675

3.3. Stability indices

3.3.1. Margin of Loss of Stability (MOLOS)

A new index is defined based on the transient energy margin in each scenario. The MOLOS index is a stability-based index evaluating the transient energy level compared to the critical energy boundary in all scenarios (success and failure) and can systematically represent the stability level of the network. The MOLOS is defined as follows:

$$\text{MOLOS} = \sum_{h=1}^{N} \frac{\Delta\mathcal{V}_h}{N}, \tag{35}$$

where $\Delta\mathcal{V}_h$ is the transient energy margin defined in (34) for the hth scenario, and N is the number of scenarios. MOLOS represents the overall system stability status, such that a larger, positive MOLOS can represent a strong system in terms of stability.

3.3.2. Risk of Instability (ROIS)

For stability-based planning purposes, a new stability-integrated reliability index is proposed based on the risk of loss of stability during the transitions. The ROIS index is a stability-based index that compares the critical and clearing energy levels in unstable transitions (failure scenarios). The ROIS is defined as follows:

$$\text{ROIS} = \left(\sum_{h=1}^{N} \frac{\Delta\mathcal{V}_h^{\text{fail}}}{N}\right)/\text{MOLOS}, \quad \forall\ \Delta\mathcal{V}_h^{\text{fail}} < -\zeta, \tag{36}$$

where $\Delta\mathcal{V}_h^{\text{fail}}$ is the transient energy margin defined in (34) for the hth failure scenario and ζ determines the risk level. There are three levels for the ζ in the ROIS index, including high-risk (HR), average-risk (AR), and risk-averse (RAV). For high-risk stability studies, ζ is equal to the minimum of the upper quartile of the absolute values of $\Delta\mathcal{V}^{\text{fail}}$ for all unstable transient scenarios. For average-risk stability studies, ζ is equal to the average of the absolute values of $\Delta\mathcal{V}^{\text{fail}}$ for all unstable transient scenarios. For risk-averse instability, ζ is equal to 0. Comparing these three parameters can help to better understand the unstable scenarios. For example, if the HR index is significantly lower than the AR index, it suggests that there are some severely unstable scenarios in the data that tend to change the average of unstable scenarios. By detecting and addressing those scenarios, a significant improvement will appear in system stability.

4. Case study

The proposed approach for integrated-stability reliability assessment for microgrids is tested on a modified version of the IEEE 33-bus system supplied by a synchronous generator and five IBRs. As shown in Fig. 3, five inverter-based resources are added at nodes 11, 18, 22, 25, and 33. The generator provides 2.42 MW with a power factor of 0.8, which is 65% of the peak load, and IBRs are responsible for supplying the rest of the loads. The reliability data of IBRs are listed in Table 1, which are taken from [31,32]. Each IBR is modeled using

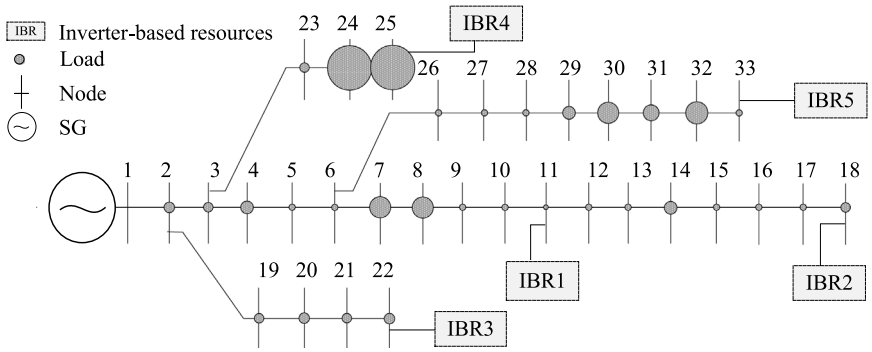

Fig. 3. IEEE 33-bus system with droop-controlled inverters supplied by a synchronous generator (SG) at bus 1.

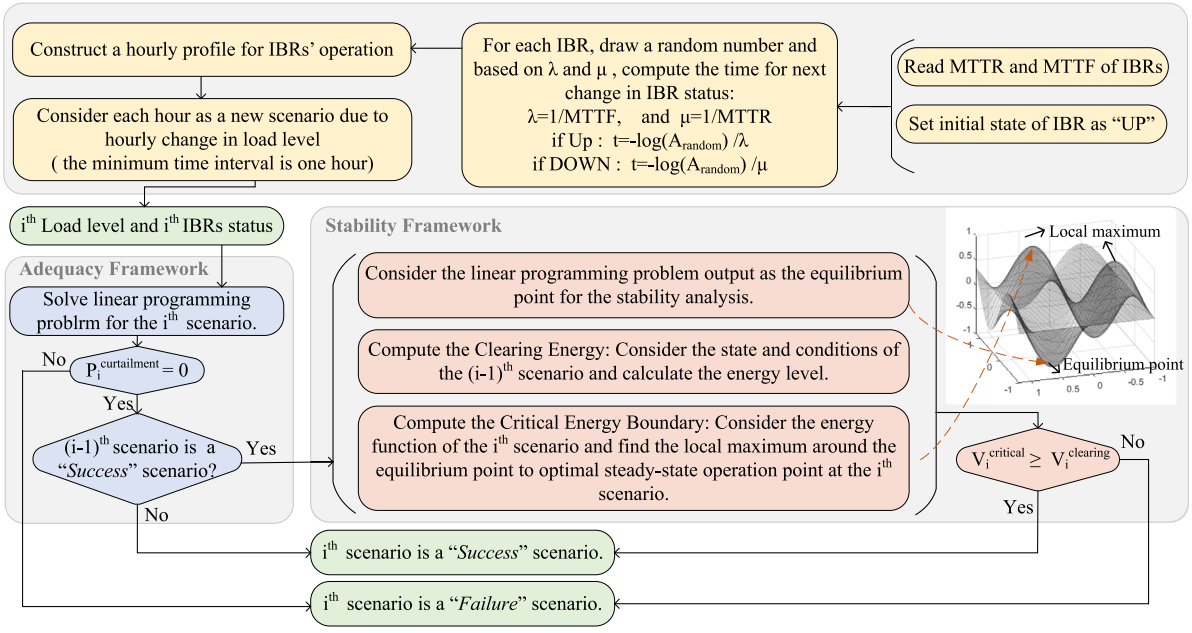

Fig. 4. Flowchart for stability integrated reliability assessment.

the droop control parameters and the second-order model described in Section 3.1.1. Moreover, load data are visualized in Fig. 3, where the sizes of gray circles represent the proportional load with respect to the system's total load. The load changes based on a yearly load profile in [33]. A small load change may not cause an unstable scenario. However, a significant alteration in system load in the islanded operating mode, especially under compromised conditions (such as when multiple IBRs are non-functional), can challenge system stability.

The sequential Monte Carlo simulation (MCS) is used to evaluate the integrated reliability and stability assessment. The linearized AC-OPF model along with MCS is used to calculate load curtailments for the reliability assessment. For the stability assessment, a transient energy function is developed for the test system based on the approach explained in Section 3.2, and the procedure for the adequacy and transient stability assessment is described in Algorithm 1 and Fig. 4. The methodologies proposed to evaluate the system's adequacy are tested using MATLAB R2023b, executed on a personal computer equipped with an Intel(R) Core i9-12900 processor and 16 GB of RAM. Additionally, the resolution of linear programming optimization problems is carried out through the sedumi solver within the MATLAB-YALMIP environment. The software and input and output are determined in Fig. 5.

For each simulated system state, the linear programming problem is solved to obtain voltage magnitudes and angles based on the defined constraints in Section 2.2 such that load curtailments are minimized. If the linear programming problem solver acquires a non-zero load curtailment for a simulated system state, the state is deemed a failure state.

If the simulated state does not result in load curtailments, the stability of the system is analyzed to determine whether the system transits stably from the previous state to this state. The linear programming problem outputs are used to find the equilibrium point (steady-state operating point), the critical energy boundaries will be determined around this point, and the previous operating point is used to compute the clearing energy. The critical boundary will be found using the Yalmip nonlinear optimizer to find the local maximum around the equilibrium point. If the clearing energy is less than the critical energy boundary, it means that the system is stable. Otherwise, the system is deemed unstable, leading to experiencing a blackout and curtailing the hourly load peak.

4.1. Result and analysis

4.1.1. Reliability indices

The reliability indices without considering the transient stability are labeled as "Inadequacy" in Table 2. The results show that calculating system inadequacy without incorporating stability assessment presents considerably smaller reliability indices. However, when transient instability cases are added to the reliability indices, these indices increase as

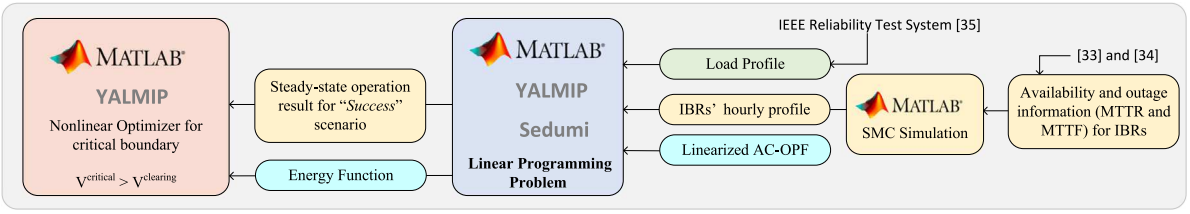

Fig. 5. Simulation and software.

Table 2
The reliability indices.

Assessment	SAIDI (h/cus.yr)	SAIFI (occ/cus.yr)	LOLP –	LOLE (h/yr)	LOLF (occ/yr)	EDNS (MW)	EENS (MWh)
Inadequacy	7.282	1.689	0.01839	161.096	32.690	0.0028	24.055
Inadequacy with Average-risk (AR) instability	19.635	4.756	0.01980	173.448	36.072	0.0076	66.243
Inadequacy with High-risk (HR) instability	23.709	5.756	0.02027	177.565	37.075	0.0092	80.154
Inadequacy with Risk-averse (RAV) instability	73.489	15.283	0.02597	22.7497	46.827	0.0258	226.104

Assume that hourly load peak is curtailed in each unstable scenario.

Algorithm 1 Proposed stability-incorporated reliability assessments algorithm

Data: Total number of scenarios, i, MTTF and MTTR for each IBR.
Result: Number of failure scenarios, i_{fail}, curtailment value at each failure scenario, number of successful scenarios, $i_{success}$.
Initialization;
– Generate the operation profile for each IBR based on their MTTF and MTTR, using sequential Monte Carlo simulation;
while *scenario* i **do**
  – Solve linear programming problem and calculate system curtailment $\rightarrow P_i^{crtl}$;
  if $P_i^{crtl} \neq 0$ **then**
    – Consider scenario i a *failure* scenario:
    $i_{fail} \leftarrow i_{fail} + 1$;
  else
    – Calculate critical energy boundary around the steady-state operating point $\rightarrow \mathcal{V}_i^{critical}$;
    – Calculate clearing energy boundary using system status in scenario $i-1 \rightarrow \mathcal{V}_{(i-1)}^{clearing}$;
    if $\mathcal{V}_i^{critical} \leq \mathcal{V}_{(i-1)}^{clearing}$ **then**
      – Consider scenario i a *failure* scenario:
      $i_{fail} \leftarrow i_{fail} + 1$;
    else
      – Consider scenario i a *successful* scenario:
      $i_{success} \leftarrow i_{success} + 1$;
    end
  end
  $i \leftarrow i - 1$;
end

Table 3
The stability indices.

	Inadequacy with AR instability	Inadequacy with HR instability	Inadequacy with RAV instability
MOLOS	–	–	123.477
ROIS (%)	−0.212	−0.228	−0.308

expected. This means that although the optimal power flow (i.e., traditional reliability evaluation) finds a feasible solution for the steady-state conditions, the network operating point cannot have a stable transition to the new steady-state operating point. In other words, during any changes, outages, faults, or disturbances, the network energy level, including kinetic and potential energies, must remain within the stability region defined by the critical energy boundary to guarantee a stable transition from one system state to another.

As proposed in Section 3.3.2, three energy margin levels are defined for labeling scenarios as being unstable: average-risk, high-risk, and risk-averse levels. As shown in Table 2, the reliability indices are also calculated based on these three levels. The value of the ζ parameter indicating average-risk level instability is greater than that indicating high-risk level instability. As a result, the reliability indices for the average-risk level are smaller than those for the high-risk level. This indicates the presence of highly unstable transitions where the clearing boundary significantly exceeds the critical energy boundary. By identifying these scenarios and improving transient stability measures accordingly, the network's average transient instability can be significantly reduced.

4.1.2. Transient stability

Two proposed stability indices, including MOLOS and ROIS, are proposed for the reliability assessment with stability criteria. The MOLOS index represents the capability of the network transient stability such that when the MOLOS value is large and positive, the average of transient energy margins ($\Delta\mathcal{V}$) is positive, and on average, the clearing energy level is smaller than critical energy boundary. On the other hand, the more negative the MOLOS is, the more likely transient instability will occur. As shown in Table 3, the MOLOS of the modified IEEE 33-bus system is large and positive, resulting in adequate network transient stability.

The other index to evaluate the stability of the system is ROIS. As described in Section 3.3.2, ROIS is a negative three-level stability index that provides information about the intensity of instability scenarios. The ROIS index shows the portion of unstable energy margin to total energy margin. As shown in Table 2, the ROIS index for high-risk level instability is close to the ROIS index for average-risk level instability. The identification and resolution of instability scenarios associated with the average risk level can lead to a substantial enhancement in the overall stability of the network. Although only 18.66% of all unstable scenarios pertain to the average risk level, effectively addressing these scenarios can result in a remarkable 74% improvement in the risk-averse ROIS. In other words, addressing the instability scenarios associated with the average risk level can have a disproportionately positive impact on the network's stability performance.

4.1.3. UISUR analysis

The reliability information of equipment and devices is determined by failure rate and repair time duration, and each unit is assumed to be equally important in overall network reliability. However, the location of the unit, integration with other adjacent units, and distributed loads at the unit node can intensify the network's unreliability. In this

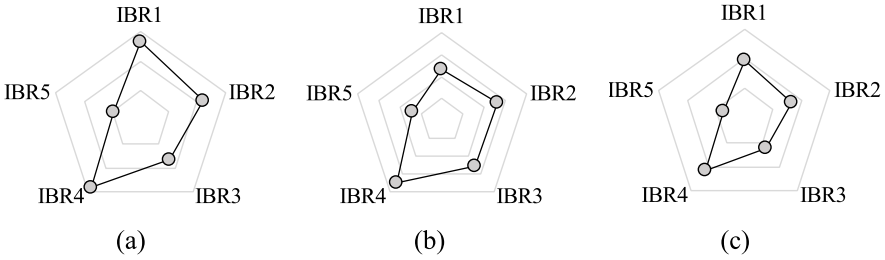

Fig. 6. UISUR analysis over (a) inadequate, (b) unstable, and (c) all scenarios.

Table 4
The UISUR index of IBRs.

IBR#	Reliability	Unstable transition	Stability-based reliability
IBR1	0.5331	0.0462	0.3910
IBR2	0.4426	0.0532	0.3291
IBR3	0.3307	0.0510	0.2491
IBR4	0.5653	0.0693	0.4354
IBR5	0.1926	0.0278	0.1450

study, the UISUR index is developed for IBR units and reported in Table 4. The UISUR is separately provided for inadequacy, instability, and stability-based reliability assessment.

Generally, the UISUR index is affected by a variety of factors including the load distribution, the MTTR and MTTF of the unit, the location of the unit, and the failure rate of neighbor units. Fig. 6 illustrates the portion of each IBR in the inadequacy, instability, and unreliability of the modified IEEE 33-bus system. IBR 4 at node 25 has a significant impact on the unreliability of the network due to several factors including responsibility for supplying two large loads at nodes 25 and 24, locating at the end of the feeder, and a high failure rate. The UISUR index of the IBR 4 proves that improving the failure rate of the unit cannot guarantee improving the reliability of the whole system. Also, the location of the unit and the neighbor loads of the unit are critical criteria for making the decision about the unit improvement.

Although IBRs 1, 2, and 3 have close MTTFs and MTTRs, the results show that they have different effects on the inadequacy and instability of the network. The capacity of IBR 1 is large, and the outage of this unit can have a certain impact on the network's inadequacy. IBR 2 at node 18 is located at the end of a long feeder, and its responsibility for compensation of voltage drop is vital. Consequently, as shown in the results, the outage of IBR 2 has a significant effect on unstable transient and overall reliability assessments.

4.2. Discussion

To conduct stability analysis using a direct method like the Lyapunov stability function, it is necessary to fulfill two primary conditions for determining the stability region: a positive Lyapunov function and a negative derivative of the Lyapunov function. At the operating point where the derivative of the Lyapunov function is zero, the Lyapunov function or energy function does not change, and identically, the system is at its steady-state operating point, named the equilibrium point of the energy function (Lyapunov function). In a traditional reliability assessment, the derivative of the energy function is indirectly investigated in each scenario by calculating the linear AC-OPF, and the calculated operating points with zero load curtailment are similar to the results of the derivative of the energy function equal to zero. Therefore, all existing methods for the reliability assessment (without any transient stability exploration) obtain only the possible equilibrium point (or feasible steady-state operating point) for the new network conditions.

Another criterion to determine a successful scenario is related to the initial operating point in each scenario where the network must transition to the new network state caused by the new contingency. In the transient stability assessment, a stable transition between two steady-state operating points is determined by comparing clearing and critical energy levels. As the results show, considering the transient instability causes the LOLP and LOLF reliability indices to increase by 0.00758 (29.19% increasing) and 13.83 (occ/yr) (30.19% increasing), respectively. Moreover, the two proposed stability-based indices, including MOLOS and ROIS, provide measures for the transient stability capability of the network. A large and positive MOLOS indicates that, on average, the modified IEEE 33-bus system experiences successful transitions during any contingencies.

The proposed three-level ROIS index classifies the risk of unstable transitions based on the energy margin ($\mathcal{V}$) and provides constructive information to improve network reliability. For example, if the high-risk ζ is smaller than the average-risk ζ of the unstable transitions, it suggests that the energy margin series of unstable transitions ($\Delta\mathcal{V}$) may be skewed toward lower values. This means that the majority of the energy margin data falls towards the lower end of the range, with a smaller proportion of higher values. From the network stability perspective, in a few scenarios, the network experiences large instability, and the energy margin is extremely negative and large; that is, the critical energy is significantly smaller than the clearing energy level. By detecting the scenarios and network conditions related to the high-risk level and addressing them, the network reliability impressively is improved.

In addition, the proposed UISUR index can provide a two-edged perspective of the direct and indirect impacts of a unit on the reliability of the network. Each unit can change the reliability assessment outcomes with its individual failure rate. Also, unit location and load distribution can affect the unit impact on the network reliability. The proposed UISUR index can help to determine the weak points of the network to have more efficient solutions to ameliorate the network reliability including both stability and inadequacy.

5. Conclusion

This paper has developed an approach for microgrid reliability assessment considering both inadequacies and instabilities. A linear programming problem is developed using a linearized AC-OPF model that includes angle, voltage, and active and reactive power and is applied to minimize load curtailments for inadequacy assessment. A new energy function based on the nonlinear dynamic model and nonlinear power flow was proposed for the transient stability assessment of the microgrid and distribution system. The energy sourced by the reactive power of the network was considered in the proposed energy function. Inverter-based resources were modeled based on the second-order dynamic model, and their droop control was also considered in the energy function. The proposed energy function is applicable to both transmission and distribution systems for transient stability assessment. A new three-level stability-based index named ROIS was proposed to evaluate the risk of instability. To have a stable system, the high-risk LOLP value should be close to the LOLP value obtained from the reliability assessment without the transient stability consideration. Also, the proposed UISUR index illustrates the impact of each unit on the overall system reliability. The outcomes underscore the significance

Table 5
The output results of the study compared with related references.

	Adequacy assessment (approach)	Stability assessment (approach)
[34–36]	✓(SMC)	✗
[37,38]	✗	✓(State-space and Linear Matrix Inequality)
[39,40]	✗	✓(Energy function in transmission system)
Proposed framework	✓(SMC)	✓(New, generalized energy function)

Based on the numerical analysis of the system presented in this study, the *adequacy analysis*, a reliability assessment without considering stability, cannot detect 29.19% of failure scenarios happening due to *unstable transition*.

of incorporating transient stability into the system reliability assessment, leading to alterations in the reliability indices. Therefore, it is crucial to consider both generation adequacy and transient stability for evaluating microgrid reliability (Table 5).

As for future work, we will extend the proposed approach to apply it on autonomously formed microgrids, which can be formed in response to major power outages or extreme events. We will also develop an approach that identifies inverter control actions that can risk-averse unstable scenarios.

CRediT authorship contribution statement

Hadis Hosseinpour: Conceptualization, Writing – original draft. **Mohammed Ben-Idris:** Conceptualization, Supervision, Writing – review & editing.

Declaration of competing interest

The authors declare the following financial interests/personal relationships which may be considered as potential competing interests: Hadis Hosseinpour reports financial support was provided by US National Science Foundation. If there are other authors, they declare that they have no known competing financial interests or personal relationships that could have appeared to influence the work reported in this paper.

Data availability

No data was used for the research described in the article.

Acknowledgment

This work was supported by the U.S. National Science Foundation (NSF) under Grant NSF ECCS-2404872.

Appendix

The energy function is constructed based on both the nonlinear AC power flow and the nonlinear dynamic model, as previously stated. However, in order to enhance the computational efficiency, we treat the equilibrium point in each scenario as identical to the steady-state operating point derived from linear programming problems and linear AC-OPF. Table 6 illustrates the discrepancy in calculating critical and clearing energy boundaries when employing the equilibrium point acquired through both linear and nonlinear AC-OPF methods, presenting a less than 1% error in the energy boundary calculations. Moreover, the simulation time for a single scenario for linear and nonlinear AC-OPF is, on average, 0.134 s and 3.964 s, respectively, representing that it reduced the computational processing time by 96.620%. For the linear AC-OPF, the *sedumi* solver is applied.

Table 6
Errors (in average) in calculating critical and clearing energy boundaries due to employing linear AC-OPF to acquire the equilibrium point.

Critical energy boundary	Clearing energy	Voltage	Angle difference
0.433%	0.055%	0.252%	2.137×10^{-5} rad

References

[1] M. Farrokhabadi, C.A. Canizares, J.W. Simpson-Porco, E. Nasr, L. Fan, P.A. Mendoza-Araya, R. Tonkoski, U. Tamrakar, N. Hatziargyriou, D. Lagos, et al., Microgrid stability definitions, analysis, and examples, IEEE Trans. Power Syst. 35 (1) (2019) 13–29.
[2] H. Farzin, M. Fotuhi-Firuzabad, M. Moeini-Aghtaie, Role of outage management strategy in reliability performance of multi-microgrid distribution systems, IEEE Trans. Power Syst. 33 (3) (2018) 2359–2369, http://dx.doi.org/10.1109/TPWRS.2017.2746180.
[3] Z. Bie, P. Zhang, G. Li, B. Hua, M. Meehan, X. Wang, Reliability evaluation of active distribution systems including microgrids, IEEE Trans. Power Syst. 27 (4) (2012) 2342–2350, http://dx.doi.org/10.1109/TPWRS.2012.2202695.
[4] I.-S. Bae, J.-O. Kim, Reliability evaluation of customers in a microgrid, IEEE Trans. Power Syst. 23 (3) (2008) 1416–1422.
[5] I.-S. Bae, J.-O. Kim, Reliability evaluation of distributed generation based on operation mode, IEEE Trans. Power Syst. 22 (2) (2007) 785–790.
[6] Y. Atwa, E.F. El-Saadany, M. Salama, R. Seethapathy, M. Assam, S. Conti, Adequacy evaluation of distribution system including wind/solar DG during different modes of operation, IEEE Trans. Power Syst. 26 (4) (2011) 1945–1952.
[7] P. Zhang, W. Li, S. Li, Y. Wang, W. Xiao, Reliability assessment of photovoltaic power systems: Review of current status and future perspectives, Appl. Energy 104 (2013) 822–833.
[8] R. Karki, R. Billinton, Reliability/cost implications of PV and wind energy utilization in small isolated power systems, IEEE Trans. Energy Convers. 16 (4) (2001) 368–373.
[9] M. Fotuhi-Firuzabad, A. Rajabi-Ghahnavie, An analytical method to consider DG impacts on distribution system reliability, in: 2005 IEEE/PES Transmission & Distribution Conference & Exposition: Asia and Pacific, IEEE, 2005, pp. 1–6.
[10] M.E. Khodayar, M. Barati, M. Shahidehpour, Integration of high reliability distribution system in microgrid operation, IEEE IEEE Trans. Smart Grid 3 (4) (2012) 1997–2006.
[11] A.K. Karngala, C. Singh, Reliability assessment framework for the distribution system including distributed energy resources, IEEE Trans. Sustain. Energy 12 (3) (2021) 1539–1548, http://dx.doi.org/10.1109/TSTE.2021.3053911.
[12] Y. Wang, V. Vittal, M. Abdi-Khorsand, C. Singh, Probabilistic reliability evaluation including adequacy and dynamic security assessment, IEEE Trans. Power Syst. 35 (1) (2019) 551–559.
[13] A.M.L. da Silva, J.L. Jardim, L.R. de Lima, Z.S. Machado, A method for ranking critical nodes in power networks including load uncertainties, IEEE Trans. Power Syst. 31 (2) (2015) 1341–1349.
[14] M. Benidris, J. Mitra, C. Singh, Integrated evaluation of reliability and stability of power systems, IEEE Trans. Power Syst. 32 (5) (2017) 4131–4139.
[15] C. Zhang, Y. Xu, Z.Y. Dong, R. Zhang, Multi-objective adaptive robust voltage/VAR control for high-PV penetrated distribution networks, IEEE IEEE Trans. Smart Grid 11 (6) (2020) 5288–5300.
[16] C. Zhang, Y. Xu, Y. Wang, Z.Y. Dong, R. Zhang, Three-stage hierarchically-coordinated voltage/var control based on PV inverters considering distribution network voltage stability, IEEE Trans. Sustain. Energy 13 (2) (2021) 868–881.
[17] K. Li, C. Shao, Z. Hu, M. Shahidehpour, An MILP method for optimal planning of electric vehicle charging stations in coordinated urban power and transportation networks, IEEE Trans. Power Syst. (2022).
[18] A. Safdarian, M. Fotuhi-Firuzabad, F. Aminifar, M. Lehtonen, A new formulation for power system reliability assessment with AC constraints, Int. J. Electr. Power Energy Syst. 56 (2014) 298–306.
[19] H. Zhu, H.J. Liu, Fast local voltage control under limited reactive power: Optimality and stability analysis, IEEE Trans. Power Syst. 31 (5) (2015) 3794–3803.
[20] H. Hosseinpour, M. MansourLakouraj, M. Ben-Idris, H. Livani, Large-signal stability analysis of inverter-based AC microgrids: A critical and analytical review, IEEE Access (2023).
[21] Q.-C. Zhong, G. Weiss, Synchronverters: Inverters that mimic synchronous generators, IEEE Trans. Ind. Electron. 58 (4) (2010) 1259–1267.
[22] F.A. Rengifo, L. Romeral, J. Cusidó, J.J. Cárdenas, New model of a converter-based generator using electrostatic synchronous machine concept, IEEE Trans. Energy Convers. 29 (2) (2014) 344–353.
[23] P.J. Hart, M. Gong, H. Liu, Z. Chen, Y. Zhang, Y. Wang, Provably-stable overload ride-through control for grid-forming inverters using system-wide Lyapunov function analysis, IEEE Trans. Energy Convers. 37 (4) (2022) 2761–2776.
[24] S. D'Arco, J.A. Suul, Virtual synchronous machines—Classification of implementations and analysis of equivalence to droop controllers for microgrids, in: 2013 IEEE Grenoble Conference, IEEE, 2013, pp. 1–7.

[25] T.M. Athay, R. Podmore, S. Virmani, A practical method for the direct analysis of transient stability, IEEE Trans. Power Appar. Syst. PAS-98 (1979) 573–584.
[26] N. Kakimoto, M. Hayashi, Transient stability analysis of multimachine power system by Lyapunov's direct method, in: 1981 20th IEEE Conference on Decision and Control Including the Symposium on Adaptive Processes, IEEE, 1981, pp. 464–470.
[27] M. Ribbens-Pavella, F. Evans, Direct methods for studying dynamics of large-scale electric power systems—A survey, Automatica 21 (1) (1985) 1–21.
[28] H. Yee, B. Spalding, Transient stability analysis of multimachine power systems by the method of hyperplanes, IEEE Trans. Power Appar. Syst. 96 (1) (1977) 276–284, http://dx.doi.org/10.1109/T-PAS.1977.32335.
[29] C.-C. Chu, H.-D. Chiang, Constructing analytical energy functions for network-preserving power system models, Circuits Systems Signal Process. 24 (4) (2005) 363–383.
[30] N. Kakimoto, Transient stability analysis of electric power system via lure-type Lyapunov function part I, Trans. IEE Japan 98 (1978) 62–71.
[31] C. Singh, J. Mitra, Monte Carlo simulation for reliability analysis of emergency and standby power systems, in: IAS'95. Conference Record of the 1995 IEEE Industry Applications Conference Thirtieth IAS Annual Meeting, Vol. 3, IEEE, 1995, pp. 2290–2295.
[32] C. Singh, P. Jirutitijaroen, J. Mitra, Electric Power Grid Reliability Evaluation: Models and Methods, John Wiley & Sons, 2018.
[33] P.M. Subcommittee, IEEE reliability test system, IEEE Trans. Power Appar. Syst. PAS-98 (6) (1979) 2047–2054, http://dx.doi.org/10.1109/TPAS.1979.319398.
[34] I.O. Guimarães, A.M.L. da Silva, L.C. Nascimento, M. Fotuhi-Firuzabad, Reliability assessment of distribution grids with DG via quasi-sequential Monte Carlo simulation, Electr. Power Syst. Res. 229 (2024) 110122.
[35] B.A. Manso, A.M. Leite da Silva, A. Milhorance, F.A. Assis, Composite reliability assessment of systems with grid-edge renewable resources via quasi-sequential Monte Carlo and cross-entropy techniques, IET Gener. Transm. Distrib. 18 (2) (2024) 326–336.
[36] D. Pandit, A. Bera, R.K. Saket, J. Mitra, N. Nguyen, Probabilistic sizing of energy storage systems for reliability and frequency security in wind-rich power grids, IEEE Trans. Ind. Appl. (2024).
[37] X. Fu, J. Sun, M. Huang, Z. Tian, H. Yan, H.H.-C. Iu, P. Hu, X. Zha, Large-signal stability of grid-forming and grid-following controls in voltage source converter: A comparative study, IEEE Trans. Power Electron. 36 (7) (2020) 7832–7840.
[38] G. San, W. Zhang, X. Guo, C. Hua, H. Xin, F. Blaabjerg, Large-disturbance stability for power-converter-dominated microgrid: A review, Renew. Sustain. Energy Rev. 127 (2020) 109859, http://dx.doi.org/10.1016/j.rser.2020.109859.
[39] T.L. Vu, K. Turitsyn, Lyapunov functions family approach to transient stability assessment, IEEE Trans. Power Syst. 31 (2) (2015) 1269–1277.
[40] D.-Z. Fang, T. Chung, Y. Zhang, W. Song, Transient stability limit conditions analysis using a corrected transient energy function approach, IEEE Trans. Power Syst. 15 (2) (2000) 804–810.